

<https://doi.org/10.1038/s42003-025-09488-5>

Aperiodic parameters of the fMRI power spectrum associate with preterm birth and neonatal age

Check for updates

Ilkka Suuronen ^{1,2,3,16} ✉, Silja Luotonen ^{1,2,3,4,16}, Henry Railo ^{1,5}, Antti Airola ⁶, Wajiha Bano ^{1,3}, Harri Merisaari ^{1,3,7}, Elmo P. Pulli ^{1,2,3}, Isabella L. C. Mariani Wigley ¹, Elena Vartiainen ^{1,3}, Niloofar Hashempour ¹, Hasse Karlsson ^{1,2,3}, Linnea Karlsson ^{1,3,8,9}, Morten L. Kringelbach ^{10,11,12}, Dafnis Batalle ^{13,14} & Jetro J. Tuulari ^{1,2,3,15}

Perinatal period is a critical time for brain development and premature-born children have an elevated likelihood for neurodevelopmental conditions. While strong associations of structural magnetic resonance imaging with preterm birth and post-menstrual age (PMA) have been reported, results with functional MRI (fMRI) have been considerably weaker. Using the task-free neonatal fMRI dataset from the Developing Human Connectome Project (dHCP), we first studied the associations of the aperiodic component of the blood-oxygen-level-dependent (BOLD) signal power spectrum from pre- and postcentral gyri with preterm birth and mapped the associations with PMA, postnatal age, and sex, and found clear differences between preterm and full-term groups, as well as males and females. Second, we used machine learning regression to predict participants' age from the aperiodic parameters of the BOLD signal from 90 cortical and subcortical regions of interest with relatively high accuracy (test R^2 's 0.20–0.41).

Brain development during gestation and after birth is rapid¹. The brain undergoes sequential, coordinated and hierarchical development that is also reflected in functional brain networks during the neonatal period and infancy². Previous work has demonstrated the presence and patterns of major brain networks' functional connectivity in fetuses³ as well as in preterm^{4–6} and term infants^{7,8}. The maturation of motor and sensory systems occurs early⁹, and in infants, cortical functional networks exhibit large confinement to primary sensory and motor areas, suggesting a perception-action task-related functional network architecture^{9,10}.

Preterm birth (birth before 37 weeks of gestation) is a common condition, occurring in about 1 in 10 births globally¹¹. It is associated with an increased likelihood for multiple adverse health outcomes in later life, including brain, cognitive, and neural impairments^{4,12–14}. Considering brain maturation, preterm birth has been associated with altered brain development as younger gestational age at birth predicts smaller brain volumes^{15–19} and higher diffusivity in the prefrontal, parietal, motor, somatosensory, and visual cortices, likely suggesting delayed maturation of these cortical areas²⁰. Prior research has also demonstrated sex-specific alterations in the preterm brain²¹. In addition to the neural correlates of preterm birth, studies have unraveled relationships of many key steps of brain development with increasing postmenstrual age (PMA) at scan²².

However, the strength of associations between PMA and brain metrics varies across imaging modalities. Structural connectivity measures have demonstrated strong correlation with PMA in neonatal subjects ($r = 0.83$)²³, as well as with gestational age in fetal subjects ($R^2 = 0.71$)²⁴, whereas functional connectivity measures have demonstrated relatively weaker correlations ($r = 0.18–0.21$)²⁵. In a recent work, however, Sun et al.²⁶ showed that both structural and functional connectomes accurately predict PMA in term and preterm infants scanned within the first months of life, although structural connectomes still had greater predictive accuracy. This underscores the potential of advanced functional imaging approaches to enhance assessments of brain maturation in neonates.

Electrophysiological activity of the brain exhibits both periodic (or oscillatory) and aperiodic (non-oscillatory) properties. The overall level of aperiodic activity, and how it changes as a function of frequency, can be modeled with two parameters: offset and exponent, respectively²⁷. The parameters change as a function of age, with the exponent decreasing in infants²⁸, and both exponent and offset decreasing during the early-childhood^{29,30} and early-adulthood³¹. Based on these EEG studies, we propose that the parameters of aperiodic brain activity could serve as markers for the pace of (functional) brain maturation. Given that aperiodic brain activity is assumed to be 'scale-free' (i.e., it is not restricted to a specific

A full list of affiliations appears at the end of the paper. ✉ e-mail: ilksuu@utu.fi

temporal scale)³², age-related changes could also be detected using aperiodic parameters of the resting-state functional MRI (rs-fMRI) blood-oxygen-level-dependent (BOLD) signal. While the utility of parameterizing brain activity in terms of its periodic and aperiodic components has been demonstrated in numerous electrophysiological studies^{27,28,33,34}, the methodology has not been widely adopted for the analysis of fMRI datasets.

An effective neurovascular coupling is already present in the developing brain before the time of normal birth³⁵, and the hemodynamic response function (HRF) can be reliably identified in neonatal participants despite being weaker in amplitude as compared to adult participants³⁶. While the aperiodic component of the fMRI BOLD signal remains relatively unexplored, evidence from concurrent multimodal measurements with electrocorticography (ECoG) and EEG connects the scale-free activity to fMRI BOLD signal response, suggesting a common neural origin^{37–39}. Wen and Liu⁴⁰ argue that whereas the periodic activity in BOLD signal supports the modular networks of the brain, the aperiodic activity is related to the global BOLD signal, which is increasingly being recognized as carrying valuable information about neuronal processes and related to various phenomena such as levels of vigilance and arousal, as well as quasi-periodic patterns of functional activity of the brain⁴¹. In neonatal participants, higher aperiodic exponents of the fMRI BOLD signal have been observed in the sensory cortex⁴², potentially suggesting local brain maturation. Although the exact origin or the significance of the aperiodic component in the fMRI BOLD signal is not yet fully understood, there is little doubt as to its origin in the neural processes of the brain, or that it carries important information relating to various processes of the brain.

In the present study, we parameterized the aperiodic components of the rs-fMRI BOLD signal power spectra (0.01–0.15 Hz) from 90 cortical and subcortical regions of interest (ROIs) in terms of their exponent and offset, using data from the dHCP neonatal rs-fMRI dataset. We then mapped the associations between the aperiodic offset and exponent parameters from the pre- and postcentral gyri and preterm birth, and postmenstrual and postnatal age, as well as sex, were included in linear mixed-effect models. Finally, we performed machine learning-based regression to predict postmenstrual and postnatal age from the aperiodic parameters from all 90 ROIs. Based on previous electrophysiological studies^{28–30,43}, particularly a recent one exploring aperiodic activity and gestational duration in neonates and toddlers⁴⁴, as well as diffusion tensor imaging studies in preterm infants²⁰, we hypothesized that postmenstrual age is positively associated, while postnatal age is negatively associated, with aperiodic parameters. Additionally, we expected preterm-born neonates to exhibit higher aperiodic parameters compared to term-born neonates, reflecting delayed neural developmental processes in the preterm group. In our statistical analysis, PMA had a statistically significant positive association with the offset of the aperiodic component, while postnatal age had a statistically significant negative association with the exponent of the aperiodic component, both in accordance with our hypothesis. Prematurity was negatively associated with the exponent with statistical significance; however, this disagrees with our hypothesis. The association between prematurity and the offset was also negative but did not reach statistical significance. Our machine learning-based elastic net regression model achieved relatively high predictive performance using aperiodic parameters as predictors, supporting the aperiodic component of the BOLD signal as a measure of brain maturation in neonatal populations.

Results and discussion

Descriptive statistics for the full sample are presented in Table 1. Descriptive statistics for the full-term and preterm subsamples are presented in Supplementary Tables S1 and S2, respectively.

The aperiodic fit was generally acceptable across the ROIs, but it was highest for somatosensory areas (Fig. 1). There was also a trend of poorer fits towards the inferior parts of the brain that may be due to poor signal-to-noise ratio in those regions⁴⁵.

Effects of postmenstrual age at scan

Postmenstrual age at scan was positively associated with the offset (Table 3: estimate = 0.06, SE = 0.01, $p < 0.001$). Further, interaction effects showed that this association was statistically significantly dependent on ROI (Table 3: estimate = 0.04, SE = 0.01, $p < 0.001$). This means that the increase of one standard deviation (SD) in child PMA predicted a +0.06 change in offset in postcentral gyri and a +0.10 change in precentral gyri.

The main effect of PMA at scan was not statistically significantly associated with the exponent, but its interaction effect with ROI was statistically significant (Table 2: estimate = -0.03, SE = 0.01, $p = 0.002$). This means that there was a crossover interaction, i.e., the association between PMA and exponent was dependent on the ROI. In postcentral gyri, the increase of one SD in child PMA predicted +0.02 change in exponent, while in precentral gyri, the corresponding change was negligible, -0.01. For the relationship between predicted aperiodic parameters and child PMA (see Supplementary Fig. S1).

During gestation, there is a proliferation of neuroblasts and synaptogenesis, ultimately leading to the capability of neurons to fire repetitive action potentials. Additionally, spontaneous neural activity begins to occur in mid-gestation (approximately at gestation week 18)^{46,47}. Given that asynchronous signals (i.e., offset) have been identified as a principal source of BOLD responses³⁸ and further, electrophysiological power shifts have been shown to be a reliable predictor of neuronal spikes⁴⁸, our results could reflect increasing neuronal firing rates as a function of postmenstrual age during gestation.

We chose the somatosensory regions for closer examination as they are known to be among the regions that mature early³. Offset values were higher in precentral compared to postcentral gyri, reflecting an elevated baseline level of BOLD signal power in the precentral gyri. Considering offset as an indirect proxy of neural activity, this suggests either higher neural activity or higher voxel-wise temporal concordance (i.e., more synchronized BOLD signal fluctuations across voxels) in the precentral (motor) gyri compared to postcentral (somatosensory) gyri. However, this difference narrows down after birth as postnatal age increases. We observed an increase in exponent values in the postcentral gyri as a function of PMA, while in the precentral gyri no noticeable change was detected. This suggests that the aperiodic activity distribution steepens in the postcentral gyri as a function of postmenstrual age. Given that in previous EEG studies flattening of the power spectrum has been linked to postnatal aging^{28–31,43}, our results could indicate earlier maturation of the precentral (motor) gyri compared to postcentral (somatosensory) gyri during gestation. This aligns with an earlier diffusion tensor imaging study of preterm newborns, which found higher fractional anisotropy and lower diffusivity in motor tracts compared to sensory tracts, reflecting earlier white matter maturation of the motor system compared to sensory pathways⁴⁹.

It is important to note that our study focused on changes in the low-frequency power spectrum of the BOLD signal (0.01–0.15 Hz), and caution is warranted when comparing our results to prior EEG literature. However, previous studies on fractional amplitude of low-frequency fluctuation (fALFF) activation in adults have reported negative correlations between age and the fALFF activation in adults^{50,51}, and fALFF activation has been demonstrated to be a valid predictor of age in children⁵². These findings suggest a trend towards less prominent low-frequency fluctuations as a function of age, also in the BOLD signal. Additionally, we found slightly higher offset values in the right hemisphere compared to the left hemisphere, indicating greater power of the BOLD signal in the right hemisphere. However, it should be noted that the difference was negligible, only 0.01. Previous studies align with our findings, suggesting earlier maturation of the right hemisphere, as cortical folding occurs earlier in the right hemisphere in fetuses. Furthermore, a general functional dominance (except for linguistic stimuli) of the right hemisphere has been described in fetuses, neonates, and preterm-born infants⁵³.

Effects of postnatal age

The negative association between the child’s postnatal age and exponent was statistically significant (Table 2: estimate = -0.17, SE = 0.03, $p < 0.001$). This association did not differ statistically significantly between the pre- and postcentral gyri, meaning that the increase of one SD in postnatal age predicts -0.17 change in exponent in both ROIs.

The negative effect of postnatal age on offset was not statistically significant. However, its interaction effect with ROI was statistically significant (Table 3: estimate = -0.02, SE = 0.01, $p = 0.048$). The result indicates that an increase of one standard deviation in postnatal age decreases the difference in offset values between the precentral and postcentral gyri by -0.02, resulting in the region-related difference disappearing at approximately 20 weeks of postnatal age. For the relationship between predicted aperiodic parameters and child postnatal age (see Supplementary Fig. S1).

Our finding of decreasing exponent values (flattening power spectrum) as a function of postnatal age is consistent with several previous EEG studies, such as a longitudinal study in infants²⁸, and several cross-sectional studies during early childhood to adolescence^{29,30}, and into early-adulthood³¹. However, these associations between age and aperiodic parameters are not necessarily linear throughout the lifespan, as McSweeney et al.⁴³ demonstrated quadratic age-related changes of offset and exponent values during childhood (in 4–11 year-olds).

Our findings suggest that after birth, in the very early stages of brain maturation, the distribution of aperiodic activity (power of BOLD signal) on different frequencies changes (flattens). This could reflect the emergence of

more widespread or global neural processes during aging, or, as discussed above, changes in brain volume or myelination. In EEG, changes in the steepness of the slope of the power spectrum have been thought to reflect cortical synaptic excitation–inhibition (E–I) balance⁵⁴, undergoing changes from the very early stages of development onwards⁵⁵. In animal studies, a steeper spectral slope (higher exponent) has been correlated to reduced E–I balance in macaque and rat cortices, possibly due to greater gamma-aminobutyric acid (GABA) synapse density⁵⁴. The aperiodic exponent has been implicated in pathology in attention deficit hyperactivity disorder (ADHD)^{56,57}, and autistic traits⁵⁸. An optimal E–I balance may play a crucial role in typical brain development, as medical treatment has been shown to lead to the “normalization” of E–I balance (exponent) in ADHD children⁵⁷. More studies examining the age-related changes of the periodic and aperiodic parameters of the fMRI BOLD signal, especially longitudinal ones, are required.

Effects of prematurity

Prematurity was negatively associated with the exponent (Table 2: estimate = -0.17, SE = 0.08, $p = 0.036$). This means that exponent values were statistically significantly smaller (-0.17 difference) in neonates born preterm compared to term-born neonates.

Prematurity was almost statistically significantly associated with offset (Table 3: estimate = -0.09, SE = 0.05, $p = 0.057$). If true, this would mean that offset values are, in general, 0.09 smaller in preterm neonates compared to term-born neonates. However, the interaction effect of prematurity and ROI was statistically significant (Table 3: estimate = 0.06, SE = 0.03, $p = 0.048$), indicating that the effect of prematurity is even weaker in precentral gyri. To see the differences in predicted aperiodic parameters between the term-born versus preterm neonates visualized (see Fig. 2).

Table 1 | Descriptive statistics for the full sample

	N	%	Mean	SD	Range
Gestational age at birth (weeks)	599		38.4	3.9	23.0–42.7
Postmenstrual age at scan (weeks)	599		40.8	2.4	27.4–44.7
Postnatal age at scan (weeks)	599		2.5	3.5	0.0–19.6
Birth weight (kg)	599		3.1	0.9	0.5–4.8
Head circumference at scan (cm)	578 ^a		34.8	2.3	21.3–39.5
DVARs z-score	599		-0.17	0.85	-2.5 to 2.3
Birth condition					
term	483	80.6			
preterm	116	19.4			
Sex					
male	323	53.9			
female	276	46.1			

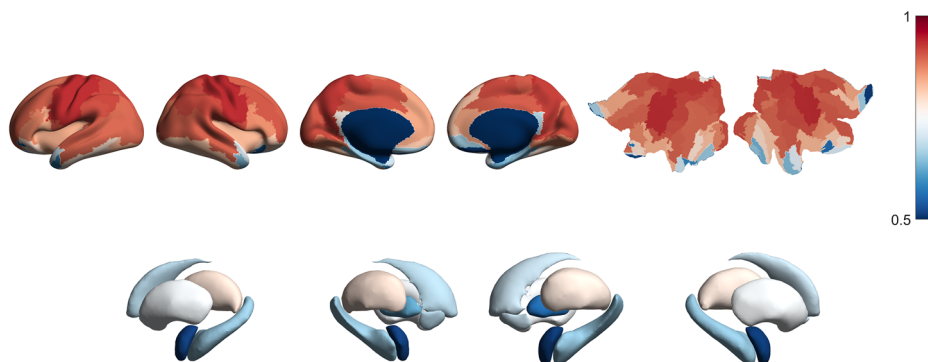
N number of participants, SD standard deviation.

^aHead circumference of 0.0 cm was reported for 21 participants, who were excluded from the computation of statistics for the corresponding row of this table.

Table 2 | Results of the linear mixed-effects regression model for exponent

	Estimate	SE	df	t value	p value
Intercept	1.89	0.03	640	69.59	<0.001
PMA at scan	0.02	0.02	611	0.87	0.385
ROI	0.01	0.01	1771	1.65	0.099
Postnatal age	-0.17	0.03	611	-6.04	<0.001
Sex	-0.09	0.03	632	-2.76	0.006
Prematurity	-0.17	0.08	631	-2.11	0.036
Hemisphere	0.01	0.01	1770	1.66	0.098
PMA at scan: ROI	-0.03	0.01	1776	-3.12	0.002
Postnatal age: ROI	-0.01	0.01	1772	-1.26	0.208
Sex: ROI	0.02	0.01	1770	1.44	0.150
Prematurity: ROI	0.03	0.03	1771	1.05	0.295

Fig. 1 | FOOOF model goodness of fit. Group mean R^2 values ($N = 599$) from the FOOOF model mapped onto cortical and subcortical regions defined by the Automated Anatomical Labeling (AAL90) atlas. The color gradient indicates the goodness of fit, with red representing higher R^2 and blue representing lower R^2 .



For the cortical and subcortical projected estimates of prematurity from the linear regression models (exponent/offset) across all 90 different brain areas (see Fig. 3). After FDR correction, the effect of prematurity on aperiodic exponent remained statistically significant only in two brain areas: right hippocampal (adjusted $p = 0.009$) and right parahippocampal (adjusted $p = 0.029$) areas. No statistically significant effects of prematurity on aperiodic offset remained in any of the brain areas. All estimates, their p -values, and FDR corrected p -values are presented in Supplementary Tables S3 and S4.

In our study, we observed smaller exponents in preterm neonates compared to term-born neonates, indicating a more flattened BOLD power distribution across frequencies. A parallel trend was seen with offsets, but the association did not reach statistical significance. Given the increasing trend in exponent values during postmenstrual aging, our findings likely reflect the shorter duration of pregnancy in preterm compared to term-born neonates. Our finding is consistent with a previous fMRI BOLD signal study demonstrating altered low-frequency fluctuation amplitudes in preterm newborns, particularly in the motor and primary sensor cortices⁵⁹. As

discussed earlier, a flattened power spectrum, at least according to prior EEG literature, may indicate a shift towards excitation, reflecting the changes in the E–I balance. Prior research has shown that preterm-born children often face a delay in inhibition abilities, though most behavioral studies suggest that they catch up with their peers by late childhood⁶⁰. Alternatively, smaller exponents may reflect more rapid postnatal neural maturational processes in preterm versus term-born neonates. Follow-up studies are needed to investigate whether the trajectory of aperiodic parameters continues to evolve throughout the lifespan.

Effects of sex

In females, aperiodic exponents were smaller (Table 2: estimate = -0.09 , SE = 0.03, $p = 0.006$) and aperiodic offsets higher compared to males (Table 3: estimate = 0.04, SE = 0.02, $p = 0.038$). No statistically significant interactions between the child's sex and ROI were found.

Sex-dependent differences in brain development have been described in previous studies, including increased functional connectivity of the visual association network in female infants²⁵ and higher fractional anisotropy in females within the posterior and temporal white matter in 5-year-olds⁶¹. Our findings align with these studies, tentatively suggesting faster brain maturation (stronger flattening of the power spectrum) in females. Further studies are needed to examine whether these sex-specific differences persist into later childhood.

Regional and hemisphere-specific differences

The offset values were higher in precentral gyri when compared to postcentral gyri (Table 3: estimate = 0.12, SE = 0.01, $p < 0.001$). There was no statistically significant association between ROI (postcentral/precentral gyri) and exponent. In the right hemisphere, offset values were negligibly 0.01 higher than in the left hemisphere (Table 3: estimate = 0.01, SE = 0.01, $p = 0.048$). Exponent values were not associated with the side of the hemisphere (right/left).

Machine learning postmenstrual and postnatal age prediction

Elastic net machine learning model performance was estimated separately using only offset-based predictors, only exponent-based predictors, and both types of predictors at once. Performance was also estimated separately

Table 3 | Results of the linear mixed-effects regression model for offset

	Estimate	SE	df	t value	p value
Intercept	-3.50	0.02	749	-209.47	<0.001
PMA at scan	0.06	0.01	653	4.07	<0.001
ROI	0.12	0.01	1795	12.16	<0.001
Postnatal age	-0.02	0.02	664	-1.42	0.156
Sex	0.04	0.02	700	2.08	0.038
Prematurity	-0.09	0.05	686	-1.91	0.057
Hemisphere	0.01	0.01	1794	1.98	0.048
PMA at scan: ROI	0.04	0.01	1799	4.88	<0.001
Postnatal age: ROI	-0.02	0.01	1794	-1.98	0.048
Sex: ROI	0.02	0.01	1793	1.87	0.062
Prematurity: ROI	0.06	0.03	1794	1.98	0.048

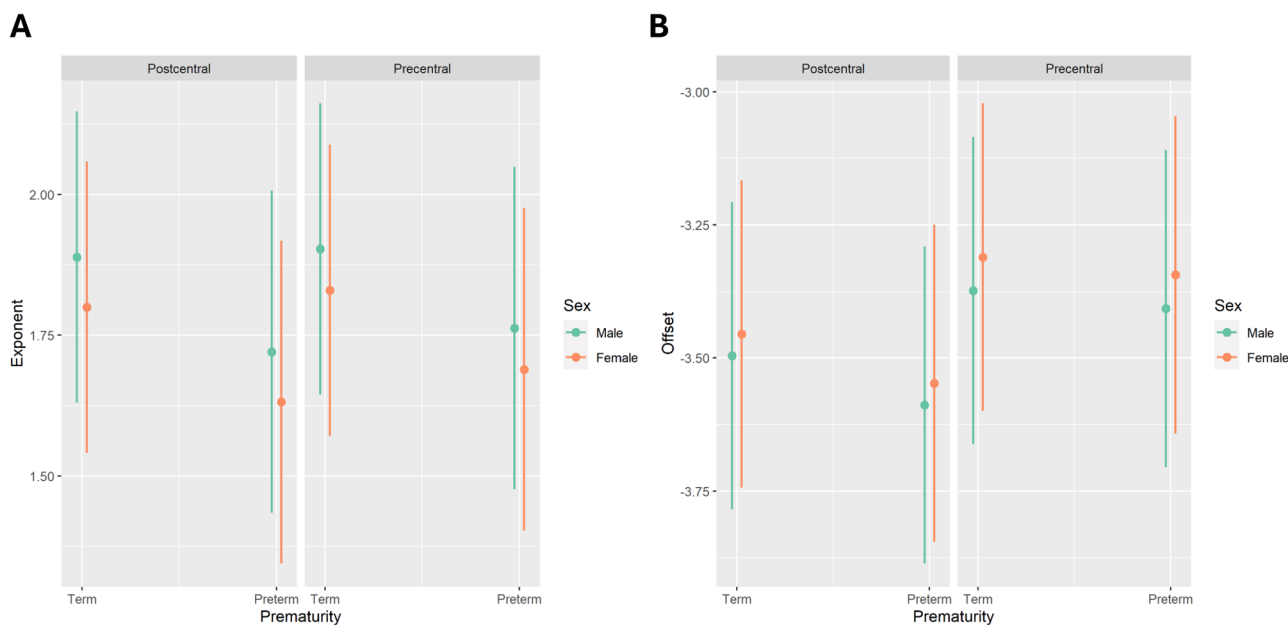
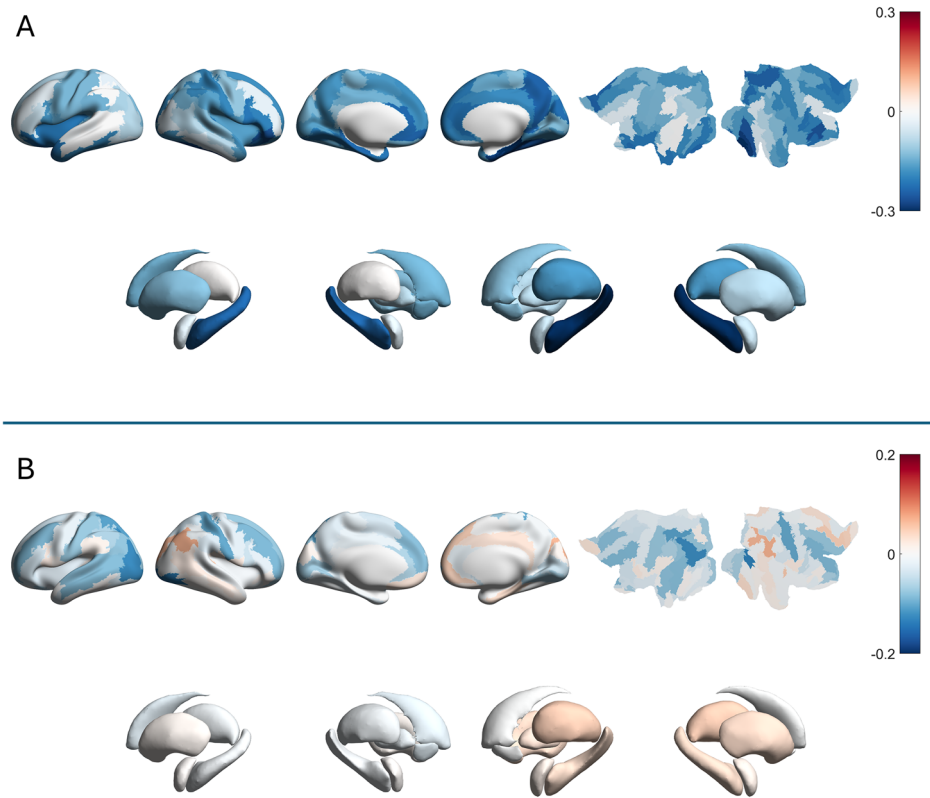


Fig. 2 | Predicted aperiodic parameters in term-born and preterm neonates by sex. Predicted values of aperiodic parameters from linear mixed-effects models for the precentral and postcentral gyri, conditioned on random effects. Green denotes males and orange denotes females. Vertical lines present 95% confidence

intervals around the average predicted value for each group **A** Aperiodic exponents ($N = 599$ biologically independent samples; 2370 observations after removal of 26 outliers). **B** Aperiodic offsets ($N = 599$ biologically independent samples; 2396 observations).

Fig. 3 | Estimates of prematurity. Linear regression estimates for prematurity (term-born = 0, pre-term = 1) mapped onto cortical and subcortical regions defined by the Automated Anatomical Labeling (AAL90) atlas. The color gradient indicates estimated magnitude (red = larger, blue = smaller). **A** Aperiodic exponent ($N = 599$). **B** Aperiodic offset ($N = 599$).



for postnatal age and PMA at the time of scan as target variables, as well as for a subset of the data containing only the term-born participants and all participants to control for the effect of preterm birth. For an estimate of the model's generalization ability, the mean values of the repeatedly cross-validated test and train set performance estimates over the cross-validation folds were reported in terms of the coefficient of determination (R^2) and the mean absolute error (MAE) in weeks of age. The performance estimates for each of the different analysis settings are presented in Tables 4–6.

The cross-validated mean performance scores associated with the different settings of input and output variables demonstrate moderate to relatively high test performance for all such settings (Test R^2 's 0.20–0.41). Offset predictors yielded generally somewhat higher performance estimates (0.24–0.36) for predicting both types of target variable than exponent predictors (0.20–0.36). The models trained with both types of predictors at once performed better than either type separately (0.24–0.41), implying that the two aperiodic parameters carry complementary information related to brain age that the model can effectively leverage for better predictive performance. As for the target variables, the models predicting postnatal age seem to perform better on term-born only subsample (0.36–0.40) as compared to full sample (0.22–0.24), whereas models predicting PMA seem to perform better on full sample (0.20–0.41) than term-only subsample (0.30–0.35), with the exception of exponent predictor model predicting PMA (0.20). Comparing mean train performance scores to test performance scores demonstrates some amount of model overfitting despite the regularization mechanism inherent to the elastic net.

For model interpretation via feature importance analysis, the mean elastic net model coefficients were computed across the cross-validation folds. Figures 4 and 5 display the mean model coefficients across cross-validation folds mapped onto cortical and subcortical regions of interest for models predicting postnatal and postmenstrual age in full-term participants, based on aperiodic exponent (Fig. 4) and offset (Fig. 5) variables. Supplementary Figs. S2 and S3 present the top-ranking positive and negative mean coefficients, while Supplementary Figs. S4–S11 present the complete reports on the model coefficients for each analysis setting.

In our machine learning data-analysis, we found that both aperiodic parameters of the BOLD signal can be used to predict neonate age with moderate to relatively high performance (R^2 's 0.20–0.41), providing support for the viability of the aperiodic component of the rs-fMRI BOLD signal as a measure of brain maturation. The offset parameter generally yielded slightly higher prediction performance estimates than the exponent parameters, and using both kinds of parameters further improved the prediction performance estimates. Previously, Kardan et al.⁶², predicted infants' postnatal age from rs-fMRI data as a regression task with high performance (median $R^2 = 0.51$), but it should be noted that the dataset differed from that of the present study, especially in that the subjects' ages were considerably higher and spanned a wider range (8–26 months). The majority of preceding studies in predicting neonate or infant age have been performed using structural^{23,63,64} or multi-modal^{65–67} MRI data. The studies focusing on predicting neonate or infant age using functional MRI are often implemented as classification tasks^{68,69}, with Smyser et al.⁶⁹ also modeling age from gestation at term age as a regression task. Regarding regional associations between rs-fMRI and age, Dosenbach et al.⁷⁰ found that the anterior prefrontal cortex and precuneus contribute most to age predictions on older subjects between 7 and 30 years. Recent efforts in machine learning based brain age prediction using the dHCP resting-state fMRI dataset, specifically, have resulted in high predictive performance (r 's = 0.42–0.69), further demonstrating the viability of a functional brain age prediction framework^{26,71}. Brain age prediction has many potential uses as a means to gain insights into normal development, and the brain age estimates in turn can be used as a predictor for various brain conditions and disorders, to be further used in the clinical context^{72,73}. Systematic bias in age estimations has, however, been reported⁷⁴, inviting for more comprehensive models to be used to avoid overestimation of age in young subjects.

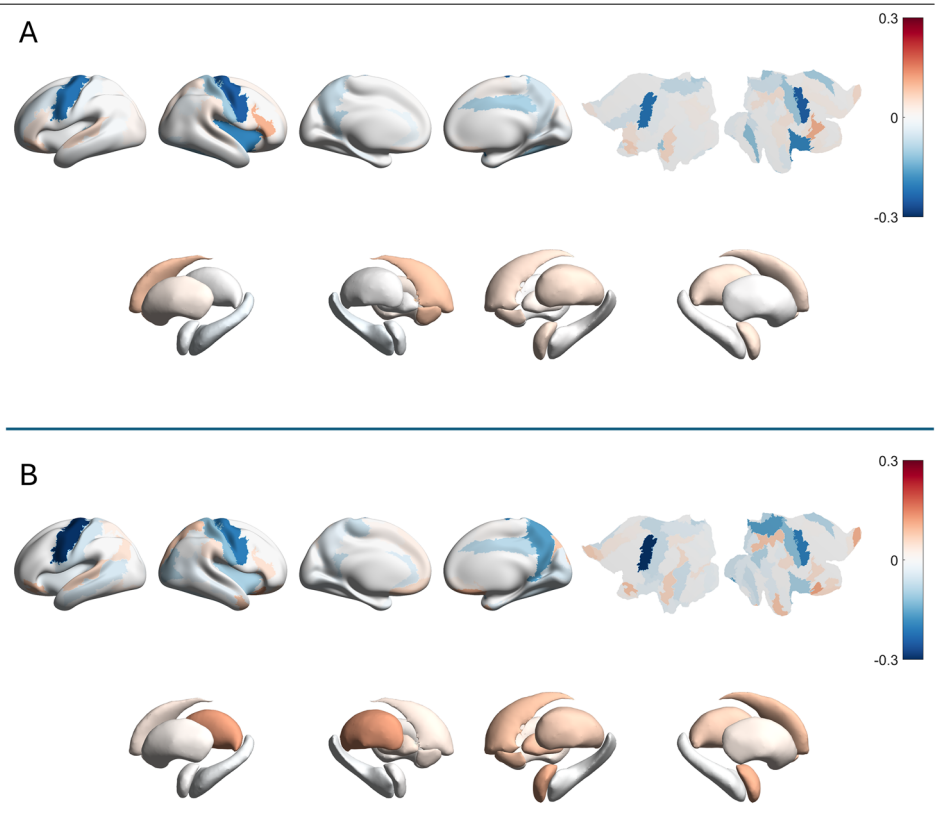
In this cross-sectional study, we used the aperiodic parameters of the BOLD signal power spectrum as a prospective index of brain maturation. Prematurity is associated with lower offsets and exponents of aperiodic activity compared to term-born neonates. This reflects a flatter distribution of aperiodic signal activity (i.e., flattening of the power spectrum) across

Table 4 | Cross-validated performance estimates for analyses predicting postnatal and postmenstrual age at scan using offset features

	Term-born postnatal	Full sample postnatal	Term-born postmenstrual	Full sample postmenstrual
Train R^2	0.50 ± 0.02	0.31 ± 0.01	0.47 ± 0.02	0.50 ± 0.02
Test R^2	0.36 ± 0.09	0.24 ± 0.12	0.32 ± 0.11	0.35 ± 0.13
Train MAE	0.74 ± 0.02	1.83 ± 0.04	0.96 ± 0.02	1.29 ± 0.03
Test MAE	0.83 ± 0.07	1.88 ± 0.26	1.07 ± 0.11	1.42 ± 0.15

Reported in terms of mean R^2 ; and MAE ± SD (in weeks). $N = 599$ neonates (483 term-born).

Fig. 4 | Elastic net coefficients for predicting age from aperiodic exponents. Mean elastic net regression coefficients over cross-validation folds for predicting age variables in term-born participants using aperiodic exponent parameters, mapped onto cortical and subcortical regions defined by the Automated Anatomical Labeling (AAL90) atlas. Color gradient indicates the magnitude of coefficients (red = larger, blue = smaller). **A** Prediction of postnatal age using exponents ($N = 483$). **B** Prediction of postmenstrual age using exponents ($N = 483$).



frequencies. The difference between preterm vs. term-born neonates was narrowly non-significant in offsets ($p = 0.057$) and significant in exponents ($p = 0.036$). The offsets were positively associated with PMA and negatively with postnatal age, while for the exponents, the association with PMA was not statistically significant, and the association with postnatal age was strongly negative. Our findings indicate an increase in aperiodic activity with postmenstrual aging, followed by a decrease in the postnatal period. Finally, in our machine learning analyses, we observed relatively strong associations (R^2 s = 0.20–0.41) between aperiodic parameters of the rs-fMRI BOLD signal and neonate age, demonstrating the feasibility of the methodology for studying functional brain maturation. The ‘conventional’ statistical testing and machine learning are complementary approaches and should not be compared directly. For instance, PMA was not associated with the exponent in the somatosensory area (Table 2), whereas in the case of elastic net regression, the exponent showed substantial prediction performance (Table 5). This is likely explained by the higher dimensionality of the data used to train the machine learning model, allowing the model to use all available information from all regions of interest, while the statistical model was limited to the preselected regions of interest.

The developing cortex exhibits spontaneous, intermittent neuronal activity, which is believed to play a critical role in the maturation and wiring of early brain networks^{75,76}. In preterm infants, these spontaneous activity

transients evolve with development and are reflected in changes in EEG measures such as decreased low-frequency power and reduced waveform variance⁷⁷. In the fMRI domain, Fransson et al.¹⁰ demonstrated that spontaneous low-frequency BOLD fluctuations in term-born infants are organized around cortical hubs, primarily located in primary sensory and motor regions. They suggested that these early hub structures could possibly gradually reorganize and expand into higher-order association networks across development.

Although the exact neural origin of low-frequency BOLD fluctuations remains unresolved, evidence from a simultaneous EEG-fMRI study in adults shows that changes in aperiodic EEG power ($1/f$ component) are coupled with hemodynamic fluctuations in auditory-salience-cerebellar and prefrontal regions³⁹. Given this cross-modal correspondence and the fact that both EEG and BOLD signals in neonates exhibit structured, non-random dynamics, it is reasonable to infer that the aperiodic component of the neonatal BOLD signal carries neurophysiologically meaningful information. The application of novel derived brain metrics to predict age parameters in neonates is a common approach to test the initial validity of the derived brain metrics^{78–80}. Nevertheless, we emphasize that this study lacks simultaneous or parallel EEG data collection that would allow us to characterize the links between EEG and fMRI aperiodic components. This remains an important topic for future studies.

Fig. 5 | Elastic net coefficients for predicting age from aperiodic offsets. Mean elastic net regression coefficients over cross-validation folds for predicting age variables in term-born participants using aperiodic offset parameters, mapped onto cortical and subcortical regions defined by the Automated Anatomical Labeling (AAL90) atlas. Color gradient indicates the magnitude of coefficients (red = larger, blue = smaller). **A** Prediction of postnatal age using offsets ($N = 483$). **B** Prediction of postmenstrual age using offsets ($N = 483$).

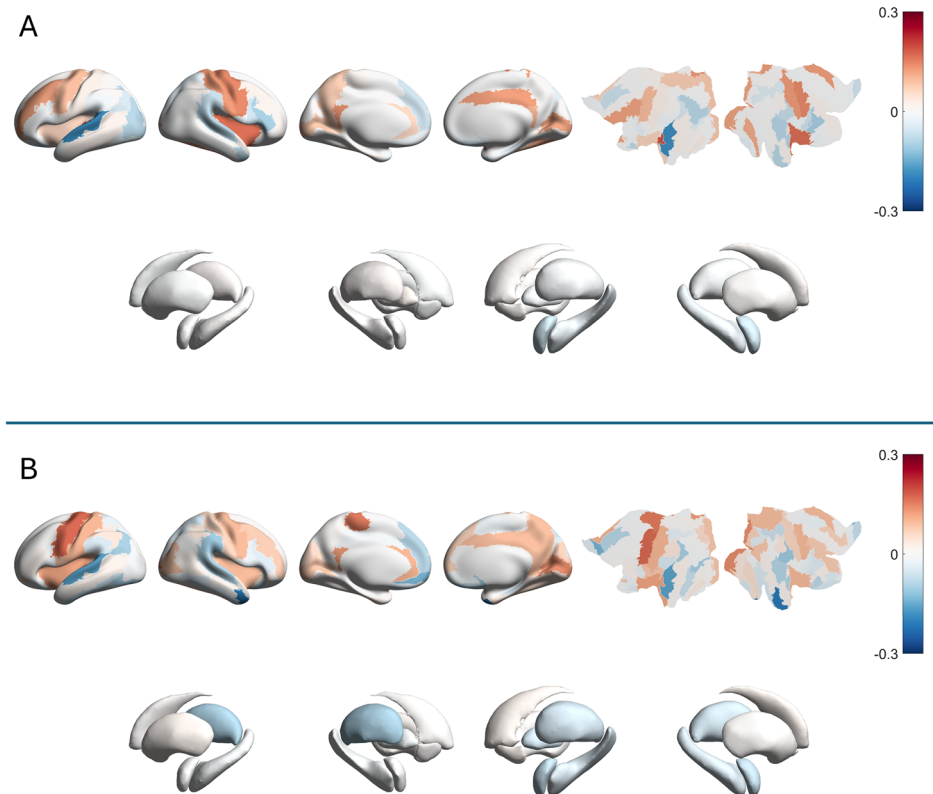


Table 5 | Cross-validated performance estimates for analyses predicting postnatal and postmenstrual age at scan using exponent features

	Term-born postnatal	Full sample postnatal	Term-born postmenstrual	Full sample postmenstrual
Train R^2	0.48 ± 0.02	0.30 ± 0.01	0.44 ± 0.01	0.39 ± 0.03
Test R^2	0.36 ± 0.10	0.22 ± 0.12	0.30 ± 0.12	0.20 ± 0.14
Train MAE	0.75 ± 0.02	1.82 ± 0.04	0.98 ± 0.01	1.37 ± 0.03
Test MAE	0.82 ± 0.07	1.89 ± 0.26	1.08 ± 0.11	1.51 ± 0.18

Reported in terms of mean R^2 ; and MAE ± SD (in weeks). $N = 599$ neonates (483 term-born)

It should be noted that our study design is cross-sectional and, therefore, no assumptions about individual changes in the pace of brain maturation can be made. However, owing to our large sample size, we are confident that our group-level findings are generalizable to a larger population. While the cross-validated test performance estimates demonstrate relatively high generalization ability of the elastic net model, it should be noted that the training performances are considerably better, implying overfitting despite model regularization⁸¹. Among newborn infants, sleep-wake patterns start to evolve soon after birth, first changing rapidly during the first few months after birth from relatively quiet and active sleep phases to structured non-rapid eye-movement and rapid eye-movement sleep^{82–84}. Their sleep is dispersed unevenly throughout the day⁸⁵, and uncertainty as to the state of wakefulness or the stage of sleep at the time of scan can complicate the interpretation of fMRI⁸⁶. Because such an effect is very difficult to avoid in this age group, we assume that changes in aperiodic parameters are related to aging, premature birth, and sex of the neonates. It has been demonstrated that functional connections strongly related to age as a target variable are more intercorrelated than expected by chance, providing redundant information, ultimately resulting in unreliable weights⁸⁷. While our study used BOLD signal parameters as features, rather than functional connections, a similar limitation may apply to the interpretability of our analysis as well. Finally, in our data set, the variation of the postnatal age in

neonates was low, due to the choice of performing the scans close to birth. This led to a highly skewed distribution of the infant age data. However, the visually inspected diagnostics of the linear regression models were acceptable.

In this study, we showed differences in aperiodic parameters of the rs-fMRI BOLD signal in preterm vs. term-born neonates and between males and females. We also demonstrated the applicability of those aperiodic parameters for the purpose of machine learning-based neonate age prediction with relatively high performance ($R^2 = 0.41$) and identified the most important ROIs to that end. Based on our results, we consider the rs-fMRI BOLD signal and its aperiodic component a viable functional brain metric for quantifying brain maturation in neonates. In addition to that, we hope that our results will enable more precise surveying of the neural origins of developmental conditions and disorders.

Methods

The present study used preprocessed data released as part of the Developing Human Connectome Project (dHCP) data release 3.0, and the methods are described in detail previously²⁵.

Research participants were prospectively recruited as part of the dHCP, an observational, cross-sectional Open Science program approved by the UK National Research Ethics Authority (14/LO/1169). Written consent was obtained from all participating families prior to imaging. All ethical

Table 6 | Cross-validated performance estimates for analyses predicting postnatal and postmenstrual age at scan using both offset and exponent features

	Term-born postnatal	Full sample postnatal	Term-born postmenstrual	Full sample postmenstrual
Train R^2	0.57 ± 0.03	0.32 ± 0.01	0.57 ± 0.05	0.67 ± 0.02
Test R^2	0.40 ± 0.09	0.24 ± 0.12	0.35 ± 0.12	0.41 ± 0.15
Train MAE	0.68 ± 0.03	1.81 ± 0.04	0.86 ± 0.05	1.04 ± 0.03
Test MAE	0.79 ± 0.07	1.87 ± 0.26	1.04 ± 0.11	1.32 ± 0.16

Reported in terms of mean R^2 and MAE ± SD (in weeks). $N = 599$ neonates (483 term-born)

regulations relevant to human research participants were followed. Term-born neonates were recruited from the postnatal wards and approached on the basis of being clinically well. Preterm-born neonates were recruited from the neonatal unit and postnatal wards. Neonates were not approached for study inclusion if there was a history of severe compromise at birth requiring prolonged resuscitation, a diagnosed chromosomal abnormality, or any contraindication to MRI scanning (e.g., due to incompatible implants). No neonates included in the final study group required treatment for a clinically significant brain injury. The third data release includes a total of 887 datasets from 783 neonates, including healthy term-born neonates, preterm neonates, and neonates at high risk for atypical neurocognitive development⁸⁸.

Participants

The openly available dHCP data set (third release) consists of 887 rs-fMRI scans from 783 neonatal research subjects between 26–45 weeks of postmenstrual age (359 females), 205 of whom were born preterm. Minor incidental findings were not considered an exclusion criterion. For a more detailed description of the data set, see Edwards et al.⁸⁸. 105 scans were flagged for failed fMRI quality control and excluded from the present analyses. Further, 129 scans were from non-singleton participants and were excluded from the present analyses to avoid indirect information leakage during cross-validation. Finally, we only included the last non-flagged scan from each participant, resulting in 605 unique, non-flagged scans from singleton participants. The spectral parameterization model fit failed for six participants, so the analyses were performed on a subset of 599 participants (276 female, PMA 27–45 weeks), 116 of them preterm-born.

fMRI data acquisition and preprocessing

The MR imaging was carried out using a 3T Philips Achieva scanner running modified Release 3.2.2 software. The length of the fMRI acquisition was 15 min and was collected with parameters: TE/TR = 38/392 ms, 2300 volumes, with an acquired spatial resolution of 2.15 mm isotropic⁸⁸. Participants were scanned non-sedated using Neonatal Brain Imaging System (NBIS), consisting of a dedicated 32-channel array coil and a positioning device⁸⁹. The functional data imaging acquisition used an optimized multiband sequence tuned for neonatal participants⁹⁰, with phase-optimized multiband pulses used throughout⁹¹. For detailed descriptions of the automated processing pipeline and the motion and distortion correction techniques applied to all dHCP open access pre-processed fMRI data, see Fitzgibbon et al.⁴⁵ and Andersson et al.^{92–95}.

Derived brain measures

An algorithmic method known as Fitting Oscillations and One-Over- F (FOOOF) for parameterizing the power spectrum into periodic and aperiodic component parameters has been suggested²⁷. While the periodic component is characterized by such parameters as its center frequency, power, and bandwidth, the $1/f$ -like aperiodic component is characterized by its offset and exponent parameters. The performance of the algorithm in characterizing neural power spectra has been validated against both simulated power spectra with known ground truth and human expert labeling on real EEG and simulated data, demonstrating a low error rate on both test arrangements²⁷.

The FOOOF algorithm parameterizes the power spectrum into its periodic and aperiodic components by creating an initial fit of the aperiodic

component and subtracting it from the total power spectrum, resulting in a flat spectrum, from which, in an iterative process, maxima are identified as peaks and used for fitting Gaussians, which are then subtracted from the flattened spectrum. When no further peaks surpassing a threshold value can be identified, a final periodic multi-Gaussian model is fit using all maxima thus identified. The periodic model is subtracted from the original spectrum, resulting in a noisy aperiodic component, to which the final aperiodic model is fit. The aperiodic component of the model is characterized by offset and exponent parameters according to the following formula:

$$L(F) = b - \log_{10}(F^X) \quad (1)$$

where F refers to frequency, b to the offset and X to the exponent parameter, which are resolved by fitting the model as described above. Notably, because the power values are presented on a logarithmic scale, negative offset values are possible. For a detailed description of the fitting procedure of the whole model, see “Algorithmic parameterization” under “Methods” in the original publication of the algorithm²⁷. For each time series representing an ROI specific BOLD signal, we estimated and parameterized the power spectrum between 0.01 and 0.15 Hz using multitaper⁹⁶ spectral analysis, and the FOOOF algorithm (Python implementation version 1.1.0), resulting in parameters for the periodic and aperiodic components of the signal, as well as an R^2 score for the goodness of fit for each ROI. For a summary on frequency range selection in earlier studies on BOLD signal, see Glerean et al.⁹⁷. In choosing the FOOOF model parameters, we did not set a maximum width for the oscillation peaks, while the minimum width of oscillatory peaks to detect was set to 0.001 Hz. Due to the sparsity of prior relevant research into the characteristics of oscillatory peaks in the rs-fMRI BOLD signal power spectrum, we used a prior work studying the rs-fMRI BOLD signal power spectrum in white matter to guide us, setting the threshold value for oscillatory peaks to 1.5 SD over the mean, as well as the maximum number of peaks to find to two⁹⁸.

Spectral parameterization of the fMRI BOLD signal was performed for 90 ROIs of the AAL90 atlas⁹⁹, encompassing both cortical and subcortical gray matter. From these regions, the precentral (motor) and postcentral (somatosensory) gyri were selected for further statistical analyses. These regions were chosen due to their early functional maturation in infancy and because the aperiodic model fit was particularly robust in these areas, with high mean R^2 values (0.94 for the precentral and 0.93 for the postcentral gyri). The pre- and postcentral gyri are located anterior and posterior to the central sulcus, respectively, and can be identified in Fig. 1 by their dark red coloring, signifying high goodness of fit. Finally, all of the regions were used in a machine learning-based regression analysis.

Linear mixed-effect regression models

Statistical analyses were performed using RStudio (2022.07.1+554) and JASP (2022, version 0.16.3). To estimate the associations between the aperiodic parameters (exponent or offset) of the fMRI BOLD signal and preterm birth, sex, PMA at scan, and postnatal age, the *lmer* function from the *afex* package of RStudio was used. Linear mixed effects regression model analyses were performed using maximum likelihood estimation. Fixed effects were PMA at scan, postnatal age, sex, and premature birth, as well as hemisphere (right/left). Interaction terms with ROI (precentral gyri/postcentral gyri) were included. In addition, in the offset model (Model 2)

exponent was included as a fixed effect to control the possible effects of exponent changes on offset values. The intercepts of subjects were modeled as random effects, including random slopes for the motion outliers. The linear mixed effects regression models had the following structure:

Model 1: Exponent \sim PMA at scan*ROI + Age*ROI + Sex*ROI + Prematurity*ROI + Hemisphere + (1 + Motion|ID)

Model 2: Offset \sim PMA at scan*ROI + Age*ROI + Sex*ROI + Prematurity*ROI + Hemisphere + Exponent + (1 + Motion | ID)

PMA at scan means the postmenstrual age (PMA) of the neonate at scan (weeks; z -transformed), and Age means the postnatal age of the child (weeks; z -transformed). Sex means the sex of the child (male = 0, female = 1), and Prematurity means term versus preterm birth (term-born = 0, preterm = 1; postmenstrual age at birth < 37 weeks). ROI means region-of-interest, either postcentral (=0) or precentral (=1) gyri, and Hemisphere means left (=0) or right (=1) side of the brain. Motion means the number of motion-compromised volumes (outliers based on DVARS; z -transformed). In Model 2, the exponent was z -transformed.

The models were originally run with only the main effects of independent variables included, but as interaction terms with ROI were added into the models, the fit of the models improved (based on lower Akaike information criterion (AIC) and statistically significant result of the likelihood ratio test before vs. after interaction term inclusion). The Prematurity variable had moderate correlation with other age variables (for the correlation matrix of all variables included in models: see Supplementary Fig. S12), but a lower AIC (when Prematurity was included) supported the inclusion of Prematurity as a predictor. Likelihood ratio test (Prematurity not included vs. included) was not statistically significant in Model 1 ($p = 0.09$) and in Model 2 ($p = 0.06$). The possibility of singularity of the models was checked and was not detected.

Further, the model assumptions were visually assessed for both models. At first, the Q-Q plot of Model 1 showed a slightly S-shaped pattern, while other visual assessments supported normal distribution of the residuals. After residual outlier detection and exclusion (± 3 SD, $N = 26$), the Q-Q plot improved. In Model 2, visual assessments supported normal distribution of the residuals, and the need for outlier exclusion was not established. For more information about model diagnostics (see Supplementary Figs. S13–S16 and Tables S5, S6).

Linear regression models

To map the estimates of *Prematurity* (term-born = 0, preterm = 1) for aperiodic parameters (exponent or offset) of fMRI BOLD signal across 90 different cortical and subcortical brain areas, the linear models following the formulas of the linear mixed effect regression models described above were used. For a more detailed description, see “Linear regression models” in the Supplementary material.

Machine learning models

We predicted the participants’ PMA and postnatal age as target variables using a supervised machine learning regression model. For each target variable, we trained and tested a regression model with either exponent, offset, or both kinds of parameters from all ROIs as predictors using a repeated and nested 10-fold cross-validation algorithm. To control for the effect of preterm birth, we trained and tested the regression models separately for the full sample and term-born only participants. In addition to the exponent and offset parameters of the aperiodic component of the power spectra of the BOLD signals, no additional predictors were introduced into the machine learning models. Performing the machine learning-based regression analysis separately using three sets of predictors (i.e., offset, exponent, and both) on two subsets (term-born only and all participants) of the data in predicting two different age target variables (postnatal and postmenstrual age at scan) resulted in 12 predictive models in total.

We used elastic net¹⁰⁰, an l1- and l2-regularized linear regression-based machine learning model to make predictions on the target variables and rank the predictors for interpretation using the model’s beta coefficients. While l1-regularized regression (aka. LASSO) performs feature selection by

enforcing sparsity, thus making the model more interpretable, it can lead to model instability if the features are highly correlated, which typically is the case with neuroimaging data⁸⁶. In contrast, elastic net accomplishes a grouping effect via l2-regularization, which is known to correct the instability-inducing tendency for arbitrary choice between correlated predictors¹⁰¹ and is considered a standard predictive algorithm in machine learning based neuroimaging studies⁸⁶. Elastic net finds the optimal model coefficients by minimizing β in the following formula:

$$\min_{\beta} \left(\frac{1}{2N} \right) \|X\beta - y\|_2^2 + \alpha * \rho |\beta|_1 + \left(\frac{\alpha(1 - \rho)}{2} \right) * |\beta|_2^2 \quad (2)$$

where β stands for the beta coefficients (aka. weights) of the model, α stands for the overall regularization strength and ρ stands for the ratio of l1-norm used in the regularization.

To estimate the models’ predictive performance on previously unseen data with low bias and variance, we used 10-times repeated 10-fold cross-validation with nested 5-fold cross-validation for the purpose of grid search-based hyperparameter tuning, the hyperparameters in question being the “ α ” and “ ρ ” in the elastic net formula (2) (i.e., “alpha” and “l1_ratio” respectively, in the scikit-learn ElasticNetCV implementation of the algorithm). The beta coefficients of the trained models were averaged over folds and ranked based on the average coefficient value for the purpose of feature importance analysis.

Prior to fitting the elastic net model, the data were standardized by subtracting the mean and scaling to unit variance—a recommended preprocessing step that is considered to have the effect of increasing the interpretability of the model⁸⁶. This preprocessing operation was performed during cross-validation in order to avoid data leakage from the test set to the model, which could occur if such preprocessing were performed prior to splitting the data.

Statistics and reproducibility

Statistical analyses were conducted using RStudio (version 2022.07.1 + 554) and JASP (version 0.16.3, 2022). No power analysis was conducted to determine sample sizes in these experiments, as the effect sizes were unknown. The sample consisted of $N = 599$ neonates. In the linear mixed-effect models, each participant contributed repeated measurements across two hemispheres (left/right) and two regions of interest (ROIs: precentral/postcentral gyri), resulting in 4 observations per subject. These repeated measures were treated as replicates, defined as multiple observations from the same subject under different anatomical conditions (ROI and hemisphere). Residual outliers (± 3 SD) were excluded where necessary (Model 1: $N = 26$ observations removed, Model 2: $N = 0$). Model comparisons were conducted using likelihood ratio tests and Akaike Information Criterion (AIC). To map the estimates of prematurity (preterm/term-born) for aperiodic parameters (exponent and offset) across all 90 cortical and subcortical regions, linear regression models were applied, and mapped effects were corrected for multiple comparisons using the false discovery rate (FDR) method.

Machine learning analyses were conducted using Python 3.8.20¹⁰² with external libraries Numpy 1.23.5¹⁰³, Pandas 2.0.3¹⁰⁴, Neurokit2 0.2.7¹⁰⁵, and Scikit-learn 1.2.2¹⁰⁶ in an interactive Jupyter notebook environment. The sample sizes for machine-learning analyses were 599 (full sample) and 483 (term-born only). The model evaluation was performed using 10-times repeated 10-fold cross-validation, and the elastic net hyperparameters (alpha and l1-ratio) were optimized using five-fold nested cross-validation. Random seed was fixed (random_state = 42) for the repeated k -fold cross-validation and the ElasticNetCV predictive model to ensure reproducibility.

Reporting summary

Further information on research design is available in the Nature Portfolio Reporting Summary linked to this article.

Data availability

The data that support the findings of this study are openly available in the National Institute of Mental Health Data Archive at https://nda.nih.gov/edit_collection.html?id=3955, reference number 3955¹⁰⁷.

Code availability

The code used in the machine learning data analysis presented in this study is available in a public repository (https://github.com/ilksuu/fmri_aperiodic_parameters_age_prediction) and archived by Zenodo¹⁰⁸. The code is released under the MIT license. Instructions for usage are provided in the README file.

Received: 4 October 2024; Accepted: 24 December 2025;

Published online: 23 January 2026

References

- Knickmeyer, R. C. et al. A structural MRI study of human brain development from birth to 2 years. *J. Neurosci.* **28**, 12176–12182 (2008).
- Gilmore, J. H., Knickmeyer, R. C. & Gao, W. Imaging structural and functional brain development in early childhood. *Nat. Rev. Neurosci.* **19**, 123–137 (2018).
- Thomason, M. E. et al. Age-related increases in long-range connectivity in fetal functional neural connectivity networks in utero. *Dev. Cogn. Neurosci.* **11**, 96–104 (2015).
- Demers, C. H. et al. Exposure to prenatal maternal distress and infant white matter neurodevelopment. *Dev. Psychopathol.* **33**, 1526–1538 (2021).
- Doria, V. et al. Emergence of resting state networks in the preterm human brain. *Proc. Natl. Acad. Sci. USA* **107**, 20015–20020 (2010).
- Smyser, C. D. et al. Longitudinal analysis of neural network development in preterm infants. *Cereb. Cortex* **20**, 2852–2862 (2010).
- Gao, W., Lin, W., Grewen, K. & Gilmore, J. H. Functional connectivity of the infant human brain: plastic and modifiable. *Neuroscientist* **23**, 169–184 (2017).
- Gao, W. et al. Evidence on the emergence of the brain's default network from 2-week-old to 2-year-old healthy pediatric subjects. *Proc. Natl. Acad. Sci. USA* **106**, 6790–6795 (2009).
- Thomason, M. E. et al. Prenatal neural origins of infant motor development: associations between fetal brain and infant motor development. *Dev. Psychopathol.* **30**, 763–772 (2018).
- Fransson, P., Aden, U., Blennow, M. & Lagercrantz, H. The functional architecture of the infant brain as revealed by resting-state fMRI. *Cereb. Cortex* **21**, 145–154 (2011).
- Walani, S. R. Global burden of preterm birth. *Int. J. Gynaecol. Obstet.* **150**, 31–33 (2020).
- Parikh, N. A. Advanced neuroimaging and its role in predicting neurodevelopmental outcomes in very preterm infants. *Semin. Perinatol.* **40**, 530–541 (2016).
- Romberg, J. et al. MRI-based brain volumes of preterm infants at term: a systematic review and meta-analysis. *Arch. Dis. Child Fetal Neonatal Ed.* **107**, 520–526 (2022).
- Allen, M. C. Neurodevelopmental outcomes of preterm infants. *Curr. Opin. Neurol.* **21**, 123 (2008).
- Inder, T. E., Warfield, S. K., Wang, H., Hüppi, P. S. & Volpe, J. J. Abnormal cerebral structure is present at term in premature infants. *Pediatrics* **115**, 286–294 (2005).
- Thompson, D. K. et al. Perinatal risk factors altering regional brain structure in the preterm infant. *Brain* **130**, 667–677 (2007).
- Parikh, N. A., Lasky, R. E., Kennedy, K. A., McDavid, G. & Tyson, J. E. Perinatal factors and regional brain volume abnormalities at term in a cohort of extremely low birth weight infants. *PLoS ONE* **8**, e62804 (2013).
- Vasu, V. et al. Preterm nutritional intake and MRI phenotype at term age: a prospective observational study. *BMJ Open* **4**, e005390 (2014).
- Alexander, B. et al. Changes in neonatal regional brain volume associated with preterm birth and perinatal factors. *Neuroimage* **185**, 654–663 (2019).
- Bouyssi-Kobar, M. et al. Regional microstructural organization of the cerebral cortex is affected by preterm birth. *Neuroimage Clin.* **18**, 871–880 (2018).
- Benavides, A. et al. Sex-specific alterations in preterm brain. *Pediatr. Res.* **85**, 55–62 (2019).
- Fenchel, D. et al. Development of microstructural and morphological cortical profiles in the neonatal brain. *Cereb. Cortex* **30**, 5767–5779 (2020).
- Taoudi-Benchekroun, Y. et al. Predicting age and clinical risk from the neonatal connectome. *Neuroimage* **257**, 119319 (2022).
- Wilson, S. et al. Development of human white matter pathways in utero over the second and third trimester. *Proc. Natl. Acad. Sci. USA* **118**, e2023598118 (2021).
- Eyre, M. et al. The Developing Human Connectome Project: typical and disrupted perinatal functional connectivity. *Brain* **144**, 2199–2213 (2021).
- Sun, H. et al. Brain age prediction and deviations from normative trajectories in the neonatal connectome. *Nat. Commun.* **15**, 10251 (2024).
- Donoghue, T. et al. Parameterizing neural power spectra into periodic and aperiodic components. *Nat. Neurosci.* **23**, 1655–1665 (2020).
- Schaworonkow, N. & Voytek, B. Longitudinal changes in aperiodic and periodic activity in electrophysiological recordings in the first seven months of life. *Dev. Cogn. Neurosci.* **47**, 100895 (2021).
- Tröndle, M., Popov, T., Dziemian, S. & Langer, N. Decomposing the role of alpha oscillations during brain maturation. *Elife* **11**, e77571 (2022).
- Hill, A. T., Clark, G. M., Bigelow, F. J., Lum, J. A. G. & Enticott, P. G. Periodic and aperiodic neural activity displays age-dependent changes across early-to-middle childhood. *Dev. Cogn. Neurosci.* **54**, 101076 (2022).
- Cellier, D., Riddle, J., Petersen, I. & Hwang, K. The development of theta and alpha neural oscillations from ages 3 to 24 years. *Dev. Cogn. Neurosci.* **50**, 100969 (2021).
- He, B. J. Scale-free brain activity: past, present and future. *Trends Cogn. Sci.* **18**, 480–487 (2014).
- Dziedo, C. A. et al. Neural and cognitive correlates of performance in dynamic multi-modal settings. *Neuropsychologia* **180**, 108483 (2023).
- Ostlund, B. et al. Spectral parameterization for studying neurodevelopment: How and why. *Dev. Cogn. Neurosci.* **54**, 101073 (2022).
- Poppe, T. et al. Neurophysiological basis of hemodynamic responses in the developing human brain before the time of normal birth. Preprint at <https://doi.org/10.1101/2022.09.23.509234> (2022).
- Arichi, T. et al. Development of BOLD signal hemodynamic responses in the human brain. *Neuroimage* **63**, 663–673 (2012).
- Miller, K. J. et al. Human motor cortical activity is selectively phase-entrained on underlying rhythms. *PLoS Comput. Biol.* **8**, e1002655 (2012).
- Winawer, J. et al. Asynchronous broadband signals are the principal source of the BOLD response in human visual cortex. *Curr. Biol.* **23**, 1145–1153 (2013).
- Jacob, M. S., Roach, B. J., Sargent, K. S., Mathalon, D. H. & Ford, J. M. Aperiodic measures of neural excitability are associated with anticorrelated hemodynamic networks at rest: a combined EEG–fMRI study. *Neuroimage* **245**, 118705 (2021).

40. Wen, H. & Liu, Z. Broadband electrophysiological dynamics contribute to global resting-state fMRI signal. *J. Neurosci.* **36**, 6030–6040 (2016).
41. Liu, T. T., Nalci, A. & Falahpour, M. The global signal in fMRI: nuisance or information?. *Neuroimage* **150**, 213–229 (2017).
42. Fransson, P. et al. Early development of spatial patterns of power-law frequency scaling in fMRI resting-state and EEG data in the newborn brain. *Cereb. Cortex* **23**, 638–646 (2013).
43. McSweeney, M. et al. Age-related trends in aperiodic EEG activity and alpha oscillations during early- to middle- childhood. *Neuroimage* **269**, 119925 (2023).
44. Luotonen, S. et al. Gestational duration and postnatal age-related changes in aperiodic and periodic parameters in neonatal and toddler electroencephalogram (EEG). *Hum. Brain Mapp.* **46**, e70130 (2025).
45. Fitzgibbon, S. P. et al. The developing Human Connectome Project (dHCP) automated resting-state functional processing framework for newborn infants. *Neuroimage* **223**, 117303 (2020).
46. Thomason, M. E. Development of brain networks in utero: relevance for common neural disorders. *Biol. Psychiatry* **88**, 40–50 (2020).
47. Cadwell, C. R., Bhaduri, A., Mostajo-Radji, M. A., Keefe, M. G. & Nowakowski, T. J. Development and arealization of the cerebral cortex. *Neuron* **103**, 980–1004 (2019).
48. Manning, J. R., Jacobs, J., Fried, I. & Kahana, M. J. Broadband shifts in local field potential power spectra are correlated with single-neuron spiking in humans. *J. Neurosci.* **29**, 13613–13620 (2009).
49. Berman, J. I. et al. Quantitative diffusion tensor MRI fiber tractography of sensorimotor white matter development in premature infants. *NeuroImage* **27**, 862–871 (2005).
50. Hu, S., Chao, H. H.-A., Zhang, S., Ide, J. S. & Li, C.-S. R. Changes in cerebral morphometry and amplitude of low-frequency fluctuations of BOLD signals during healthy aging: correlation with inhibitory control. *Brain Struct. Funct.* **219**, 983–994 (2014).
51. Montalà-Flaquer, M. et al. Spontaneous brain activity in healthy aging: an overview through fluctuations and regional homogeneity. *Front. Aging Neurosci.* **14**, 1002811 (2022).
52. Sato, J. R. et al. Default mode network maturation and psychopathology in children and adolescents. *J. Child Psychol. Psychiatry* **57**, 55–64 (2016).
53. Bisiacchi, P. & Cainelli, E. Structural and functional brain asymmetries in the early phases of life: a scoping review. *Brain Struct. Funct.* **227**, 479–496 (2022).
54. Gao, R., Peterson, E. J. & Voytek, B. Inferring synaptic excitation/inhibition balance from field potentials. *NeuroImage* **158**, 70–78 (2017).
55. Zhang, Z., Jiao, Y.-Y. & Sun, Q.-Q. Developmental maturation of excitation and inhibition balance in principal neurons across four layers of somatosensory cortex. *Neuroscience* **174**, 10–25 (2011).
56. Karalunas, S. L. et al. Electroencephalogram aperiodic power spectral slope can be reliably measured and predicts ADHD risk in early development. *Dev. Psychobiol.* **64**, e22228 (2022).
57. Robertson, M. M. et al. EEG power spectral slope differs by ADHD status and stimulant medication exposure in early childhood. *J. Neurophysiol.* **122**, 2427–2437 (2019).
58. Carter Leno, V. et al. Infant excitation/inhibition balance interacts with executive attention to predict autistic traits in childhood. *Mol. Autism* **13**, 46 (2022).
59. Wu, X. et al. Frequency of spontaneous BOLD signal differences between moderate and late preterm newborns and term newborns. *Neurotox. Res.* **30**, 539–551 (2016).
60. Réveillon, M., Hüppi, P. S. & Barisnikov, K. Inhibition difficulties in preterm children: developmental delay or persistent deficit?. *Child Neuropsychol.* **24**, 734–762 (2018).
61. Kumpulainen, V. et al. Sex differences, asymmetry, and age-related white matter development in infants and 5-year-olds as assessed with tract-based spatial statistics. *Hum. Brain Mapp.* **44**, 2712–2725 (2023).
62. Kardan, O. et al. Resting-state functional connectivity identifies individuals and predicts age in 8-to-26-month-olds. *Dev. Cogn. Neurosci.* **56**, 101123 (2022).
63. Hong, J. et al. Brain age prediction of children using routine brain MR images via deep learning. *Front. Neurol.* **11**, 584682 (2020).
64. Chen, J. V. et al. Deep learning to predict neonatal and infant brain age from myelination on brain MRI scans. *Radiology* **305**, 678–687 (2022).
65. Galdi, P. et al. Neonatal morphometric similarity mapping for predicting brain age and characterizing neuroanatomic variation associated with preterm birth. *Neuroimage Clin.* **25**, 102195 (2020).
66. Hu, D. et al. Disentangled-multimodal adversarial autoencoder: application to infant age prediction with incomplete multimodal neuroimages. *IEEE Trans. Med. Imaging* **39**, 4137–4149 (2020).
67. Liem, F. et al. Predicting brain-age from multimodal imaging data captures cognitive impairment. *Neuroimage* **148**, 179–188 (2017).
68. Pruett, J. R. et al. Accurate age classification of 6 and 12 month-old infants based on resting-state functional connectivity magnetic resonance imaging data. *Dev. Cogn. Neurosci.* **12**, 123–133 (2015).
69. Smyser, C. D. et al. Prediction of brain maturity in infants using machine-learning algorithms. *Neuroimage* **136**, 1–9 (2016).
70. Dosenbach, N. U. F. et al. Prediction of individual brain maturity using fMRI. *Science* **329**, 1358–1361 (2010).
71. Kim, J.-H., De Asis-Cruz, J. & Limperopoulos, C. Separating group- and individual-level brain signatures in the newborn functional connectome: a deep learning approach. *Neuroimage* **299**, 120806 (2024).
72. Mishra, S., Beheshti, I. & Khanna, P. A review of neuroimaging-driven brain age estimation for identification of brain disorders and health conditions. *IEEE Rev. Biomed. Eng.* **16**, 371–385 (2023).
73. Bass, C. et al. ICAM-Reg: Interpretable Classification and Regression with feature attribution for mapping neurological phenotypes in individual scans. *IEEE Trans. Med. Imaging* **42**, 959–970 (2023).
74. Liang, H., Zhang, F. & Niu, X. Investigating systematic bias in brain age estimation with application to post-traumatic stress disorders. *Hum. Brain Mapp.* **40**, 3143–3152 (2019).
75. O'Donovan, M. J. The origin of spontaneous activity in developing networks of the vertebrate nervous system. *Curr. Opin. Neurobiol.* **9**, 94–104 (1999).
76. Vanhatalo, S. & Kaila, K. Development of neonatal EEG activity: from phenomenology to physiology. *Semin. Fetal Neonatal Med.* **11**, 471–478 (2006).
77. Tolonen, M., Palva, J. M., Andersson, S. & Vanhatalo, S. Development of the spontaneous activity transients and ongoing cortical activity in human preterm babies. *Neuroscience* **145**, 997–1006 (2007).
78. Fair, D. A. et al. The maturing architecture of the brain's default network. *Proc. Natl. Acad. Sci. USA* **105**, 4028–4032 (2008).
79. Alcauter, S. et al. Frequency of spontaneous BOLD signal shifts during infancy and correlates with cognitive performance. *Dev. Cogn. Neurosci.* **12**, 40–50 (2015).
80. França, L. G. S. et al. Neonatal brain dynamic functional connectivity in term and preterm infants and its association with early childhood neurodevelopment. *Nat Commun.* **15**, 16 (2024).
81. Nielsen, A. N., Barch, D. M., Petersen, S. E., Schlaggar, B. L. & Greene, D. J. Machine learning with neuroimaging: evaluating its applications in psychiatry. *Biol. Psychiatry Cogn. Neurosci. Neuroimaging* **5**, 791–798 (2020).
82. Louis, J., Cannard, C., Bastuji, H. & Challamel, M. J. Sleep ontogenesis revisited: a longitudinal 24-hour home polygraphic study on 15 normal infants during the first two years of life. *Sleep* **20**, 323–333 (1997).

83. Ficca, G., Fagioli, I. & Salzarulo, P. Sleep organization in the first year of life: developmental trends in the quiet sleep–paradoxical sleep cycle. *J. Sleep. Res.* **9**, 1–4 (2000).
84. Coons, S. & Guilleminault, C. Development of sleep–wake patterns and non-rapid eye movement sleep stages during the first six months of life in normal infants. *Pediatrics* **69**, 793–798 (1982).
85. Rivkees, S. A. Developing circadian rhythmicity in infants. *Pediatrics* **112**, 373–381 (2003).
86. Scheinost, D. et al. Machine learning and prediction in fetal, infant, and toddler neuroimaging: a review and primer. *Biol. Psychiatry* **93**, 893–904 (2023).
87. Pathania, A., Schreiber, M., Miller, M. W., Euler, M. J. & Lohse, K. R. Exploring the reliability and sensitivity of the EEG power spectrum as a biomarker. *Int. J. Psychophysiol.* **160**, 18–27 (2021).
88. Edwards, A. D. et al. The Developing Human Connectome Project neonatal data release. *Front. Neurosci.* **16**, 886772 (2022).
89. Hughes, E. J. et al. A dedicated neonatal brain imaging system. *Magn. Reson. Med.* **78**, 794–804 (2017).
90. Price, A. N. et al. *Accelerated Neonatal fMRI using Multiband EPI* 3911 (ISMRM, 2015).
91. Malik, S. J., Price, A. N. & Hajnal, J. V. Optimized amplitude modulated multi-band RF pulses. In *Proc. of the ISMRM 2015* 2398 (2015).
92. Andersson, J. L., Hutton, C., Ashburner, J., Turner, R. & Friston, K. Modeling geometric deformations in EPI time series. *Neuroimage* **13**, 903–919 (2001).
93. Andersson, J. L. R., Skare, S. & Ashburner, J. How to correct susceptibility distortions in spin-echo echo-planar images: application to diffusion tensor imaging. *Neuroimage* **20**, 870–888 (2003).
94. Andersson, J. L. R. et al. Towards a comprehensive framework for movement and distortion correction of diffusion MR images: within volume movement. *Neuroimage* **152**, 450–466 (2017).
95. Andersson, J. L. R., Graham, M. S., Drobnyak, I., Zhang, H. & Campbell, J. Susceptibility-induced distortion that varies due to motion: correction in diffusion MR without acquiring additional data. *Neuroimage* **171**, 277–295 (2018).
96. Thomson, D. J. Spectrum estimation and harmonic analysis. *Proc. IEEE* **70**, 1055–1096 (1982).
97. Glerean, E., Salmi, J., Lahnakoski, J. M., Jääskeläinen, I. P. & Sams, M. Functional magnetic resonance imaging phase synchronization as a measure of dynamic functional connectivity. *Brain Connect.* **2**, 91–101 (2012).
98. Li, M., Gao, Y., Ding, Z. & Gore, J. C. Power spectra reveal distinct BOLD resting-state time courses in white matter. *Proc. Natl. Acad. Sci. USA* **118**, e2103104118 (2021).
99. Tzourio-Mazoyer, N. et al. Automated anatomical labeling of activations in SPM using a macroscopic anatomical parcellation of the MNI MRI single-subject brain. *Neuroimage* **15**, 273–289 (2002).
100. Zou, H. & Hastie, T. Regularization and variable selection via the elastic net. *J. R. Stat. Soc. Ser. B (Stat. Methodol.)* **67**, 301–320 (2005).
101. Zhou, D.-X. On grouping effect of elastic net. *Stat. Probab. Lett.* **83**, 2108–2112 (2013).
102. Rossum, G. V. & Drake, F. L. *The Python Language Reference Manual* (Network Theory Limited, 2011).
103. Harris et al. Array programming with NumPy. *Nature* **585**, 357–362 (2020).
104. McKinney, W. *Data Structures for Statistical Computing in Python* 56–61 <https://doi.org/10.25080/Majora-92bf1922-00a> (2010).
105. Makowski, D. et al. NeuroKit2: a Python toolbox for neurophysiological signal processing. *Behav. Res.* **53**, 1689–1696 (2021).
106. Pedregosa, F. et al. Scikit-learn: machine learning in Python. *J. Mach. Learn. Res.* **12**, 2825–2830 (2011).
107. Edwards, D., Hajnal, J., Rueckert, D. & Smith, S. Developing Human Connectome Project (dHCP) data collection. *NIMH Data Archive* <https://doi.org/10.15154/92vw-g837> (2021).
108. Suuronen, I. ilksuu/fmri_aperiodic_parameters_age_prediction: aperiodic parameters of the fMRI power spectrum associate with preterm birth and neonatal age. *Zenodo* <https://doi.org/10.5281/ZENODO.17903944> (2025).

Acknowledgements

Data were provided by the developing Human Connectome Project, KCL-Imperial-Oxford Consortium funded by the European Research Council under the European Union Seventh Framework Program (FP/2007–2013)/ERC Grant Agreement no. [319456]. We are grateful to the families who generously supported this trial. Authors have received funding from the following sources: Ilkka Suuronen, Emil Aaltonen Foundation, Sigrid Jusélius Foundation, Silja Luotonen, The Finnish Cultural Foundation/Varsinais-Suomi Regional Fund, Signe & Ane Gyllenberg Foundation, Elmo P. Pulli, Emil Aaltonen Foundation, Juho Vainio Foundation, Päivikki and Sakari Sohlberg Foundation, Finnish Brain Foundation, The Finnish Cultural Foundation, Strategic Research Council (SRC) established within the Research Council of Finland (#352648 and subproject #352655), Signe and Ane Gyllenberg foundation, Niloofer Hashempour, University of Turku Graduate School, Jetro J. Tuulari, Finnish Medical Foundation, Emil Aaltonen Foundation, Sigrid Jusélius Foundation, Signe and Ane Gyllenberg Foundation, Hospital District of Southwest Finland State Research Grants, Harri Merisaari, Academy of Finland (#26080983), Henry Railo, Academy of Finland (#351109), Dafnis Batalle. D.B. acknowledges support from a Wellcome Trust Seed Award in Science [217316/Z/19/Z], and support in part from the Institute for Translational Neurodevelopment at King’s College London, and the NIHR Maudsley Biomedical Research Centre at South London and Maudsley NHS Foundation Trust and King’s College London. The views expressed are those of the authors and not necessarily those of the NHS, the National Institute for Health Research (NIHR), or the Department of Health and Social Care. The funders had no role in the design and conduct of the study; collection, management, analysis, and interpretation of the data; preparation, review, or approval of the manuscript; and decision to submit the manuscript for publication.

Author contributions

J.J.T. conceived the project. I.S. and S.L. designed and performed the data analysis and contributed equally to the manuscript with input from all authors (H.R., A.A., W.B., H.M., E.P.P., I.M., E.V., N.H., H.K., L.K., M.L.K., D.B., and J.J.T.). All authors reviewed and approved the final manuscript.

Competing interests

The authors declare no competing interests.

Additional information

Supplementary information The online version contains supplementary material available at <https://doi.org/10.1038/s42003-025-09488-5>.

Correspondence and requests for materials should be addressed to Ilkka Suuronen.

Peer review information *Communications Biology* thanks Junghoon Kim and Huili Sun for their contribution to the peer review of this work. Primary Handling Editors: Sahar Ahmad and Jasmine Pan.

Reprints and permissions information is available at <http://www.nature.com/reprints>

Publisher’s note Springer Nature remains neutral with regard to jurisdictional claims in published maps and institutional affiliations.

Open Access This article is licensed under a Creative Commons Attribution-NonCommercial-NoDerivatives 4.0 International License, which permits any non-commercial use, sharing, distribution and reproduction in any medium or format, as long as you give appropriate credit to the original author(s) and the source, provide a link to the Creative Commons licence, and indicate if you modified the licensed material. You do not have permission under this licence to share adapted material derived from this article or parts of it. The images or other third party material in this article are included in the article's Creative Commons licence, unless indicated otherwise in a credit line to the material. If material is not included in the article's Creative Commons licence and your intended use is not permitted by statutory regulation or exceeds the permitted use, you will need to obtain permission directly from the copyright holder. To view a copy of this licence, visit <http://creativecommons.org/licenses/by-nc-nd/4.0/>.

© The Author(s) 2026

¹FinnBrain Birth Cohort Study, Department of Clinical Medicine, Turku Brain and Mind Center, University of Turku, Turku, Finland. ²Department of Psychiatry, Turku University Hospital and University of Turku, Turku, Finland. ³Centre for Population Health Research, Turku University Hospital and University of Turku, Turku, Finland. ⁴Department of Pediatric Neurology, Turku University Hospital, University of Turku, Turku, Finland. ⁵Department of Psychology and Speech Language Pathology, University of Turku, Turku, Finland. ⁶Department of Computing, University of Turku, Turku, Finland. ⁷Department of Diagnostic Radiology, University of Turku, Turku, Finland. ⁸Department of Clinical Medicine, Unit of Public Health, University of Turku, Turku, Finland. ⁹Department of Child Psychiatry, Turku University Hospital, Turku, Finland. ¹⁰Centre for Eudaimonia and Human Flourishing, Linacre College, University of Oxford, Oxford, UK. ¹¹Department of Psychiatry, University of Oxford, Oxford, UK. ¹²Center for Music in the Brain, Department of Clinical Medicine, Aarhus University, Aarhus, Denmark. ¹³Department of Forensic and Neurodevelopmental Sciences, Institute of Psychiatry, Psychology & Neuroscience, King's College London, London, UK. ¹⁴Department of Early Life Imaging, School of Biomedical Engineering and Imaging Sciences, King's College London, London, UK. ¹⁵Turku Collegium for Science, Medicine and Technology, University of Turku, Turku, Finland. ¹⁶These authors contributed equally: Ilkka Suuronen, Silja Luotonen. ✉ e-mail: ilksuu@utu.fi